lymerized as a result of a steric barrier or an unfavorable lattice matching. In this case, a dark band defines one folding unit.

REFERENCES

1. M. Sano, D. Y. Sasaki, T. Kunitake, *J. Chem. Soc., Chem. Commun.*, in press.
2. M. Sano, D. Y. Sasaki, T. Kunitake, *Macromolecules*, in press.
3. _____, *Proc. Jpn. Acad. B* **68**, 87 (1992).
4. H. K. Hall, Jr., *J. Am. Chem. Soc.* **80**, 6404 (1959).
5. M. Sano and T. Kunitake, *J. Vac. Sci. Technol. B* **9**, 1137 (1991).
6. G. C. McGonigal, R. H. Bernhardt, D. J. Thomson, *Appl. Phys. Lett.* **57**, 28 (1990).
7. D. R. Holmes, C. W. Bunn, D. J. Smith, *J. Polym. Sci.* **17**, 159 (1955).
8. H. Arimoto, M. Ishibashi, M. Hirai, Y. Chatani, *J. Polym. Sci. A* **3**, 317 (1965).
9. P. R. Baukema and A. J. Hopfinger, *J. Polym. Sci. Polym. Phys. Ed.* **20**, 399 (1982).
10. J. Willems, *Experientia* **23**, 409 (1967).
11. A. J. Groszek, *Proc. R. Soc. London Ser. A* **314**, 473 (1970).
12. For liquid crystals, see, for example, D. P. E. Smith, J. K. H. Hörber, G. Binnig, H. Nejoh, *Nature* **344**, 641 (1990).
13. J. J. Novoa and M.-H. Whangbo, *J. Am. Chem. Soc.* **113**, 9017 (1991).

14 May 1992; accepted 20 July 1992

Small-Angle Synchrotron X-ray Scattering Reveals Distinct Shape Changes of the Myosin Head During Hydrolysis of ATP

Katsuzo Wakabayashi, Makio Tokunaga, Izumi Kohno, Yasunobu Sugimoto, Toshiaki Hamanaka, Yasunori Takezawa, Takeyuki Wakabayashi, Yoshiyuki Amemiya

In the energy transduction of muscle contraction, it is important to know the nature and extent of conformational changes of the head portion of the myosin molecules. In the presence of magnesium adenosine triphosphate (MgATP), fairly large conformational changes of the myosin head [subfragment-1 (S1)] in solution were observed by small-angle x-ray scattering with the use of synchrotron radiation as an intense and stable x-ray source. The presence of MgATP reduced the radius of gyration of the molecule by about 3 angstrom units and the maximum chord length by about 10 angstroms, showing that the shape of S1 becomes more compact or round during hydrolysis of MgATP. Comparison with various nucleotide-bound S1 complexes that correspond to the known intermediate states during ATP hydrolysis indicates that the shape of S1 in a key intermediate state, S1-bound adenosine diphosphate (ADP) and phosphate [S1.ADP.P_i], differs significantly from the shape in the other intermediate states of the S1 adenosine triphosphatase cycle as well as that of nucleotide-free S1.**

Conformational changes of the myosin head have been widely investigated because of their possible role in the molecular mechanism of muscle contraction and other myosin-driven motile systems. In vitro motility assays in which the head alone was used strongly suggest that internal motions of the myosin head play an important role in the sliding movement of the actin filaments (*1*). Many physicochemical studies [see, for example, (*2*, *3*)] have indicated that changes of the myosin head occur during hydrolysis of ATP. Such conformational changes have been attributed to the internal flexibility of the head (*3*). Recent electron microscopy (EM) studies, in conjunction with ATP hydrolysis, have revealed the possibility of comparatively large shape changes of the head both for the isolated myosin (*4*) and actin-S1 complexes (*5*, *6*). In contrast, previous x-ray and neutron small-angle scattering studies have not shown a distinct change in the head structure on binding of nucleotide (an ATP analog) (*7*) or on "invisible" F-actin (*8*), suggesting that no significant change occurs in the head during activity.

In this report we present direct evidence for a structural change in the myosin head (S1) during active hydrolysis of MgATP. Improved methods of small-angle x-ray scattering were used with synchrotron radiation as an intense and stable x-ray source. The correlation between changes in the S1 structure and biochemical states thought to be part of the S1 adenosine triphosphatase (ATPase) cycle was determined.

Papain-treated chicken S1 [molecular mass 130 kD (*9*)], which has a full component of the light chains (*10*, *11*), was used immediately after purification by gel filtration, and only peak fractions were retained. A series of x-ray measurements on nucleotide-free and various nucleotide-bound S1 complexes were made with the use of an exposure time of 3 min at 18.5°C (*12*). Protein concentrations were varied from 3 to 7 mg/ml. X-ray measurements on S1 in the presence of 5 mM MgATP were started within 0.5 min after S1 was mixed with ATP. Because the rate constant of MgATP hydrolysis by S1 in solution is ~0.05 s^{-1} at room temperature (*13*), most of the ATP (at least 4 mmol) should remain unhydrolyzed at the end of the x-ray measurement.

Small-angle x-ray scattering curves are presented in Fig. 1 as Guinier plots {ln[$I(S)$] versus S^2 plots} (*14*), where $I(S)$ is the scattered x-ray intensity and $S = 2\sin\theta/\lambda$ (where 2θ is the scattering angle and λ is the x-ray wavelength). The Guinier plots from all S1 samples gave straight lines in the range of $S^2 \leq 0.223 \times 10^{-4}$ Å^{-2} (S^2_{max}), and there was no evidence of upward curvature at lower values of S^2 that would have resulted from aggregation of the molecules in solution (*14*, *15*). The straight region (the Guinier region) was narrow,

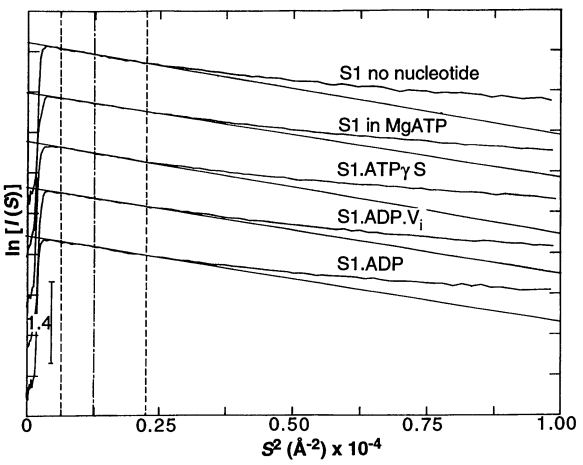

Fig. 1. Typical small-angle x-ray scattering curves of various S1 samples on a Guinier plot. These plots are 7 mg/ml data. The straight lines represent extrapolated Guinier fits. The fitting ranges (the Guinier regions) of the straight lines are indicated by vertical dashed lines [$S^2 = 0.0778 \times 10^{-4}$ Å^{-2} (S^2_{min}) and $S^2 = 0.2228 \times 10^{-4}$ Å^{-2} (S^2_{max})]. The dotted chain line at 0.12×10^{-4} Å^{-2} shows the S^2 value of the present Guinier's criterion (*21*). For clarity, the curves have been shifted successively by 0.8 unit on the ln[$I(S)$] axis.

K. Wakabayashi, I. Kohno, Y. Sugimoto, T. Hamanaka, Y. Takezawa, Department of Biophysical Engineering, Faculty of Engineering Science, Osaka University, Toyonaka, Osaka 560, Japan.
M. Tokunaga and T. Wakabayashi, Department of Physics, Faculty of Science, University of Tokyo, Bunkyo-ku, Tokyo 113, Japan.
Y. Amemiya, the Photon Factory, National Laboratory for High Energy Physics, Tsukuba, Ibaraki 305, Japan.

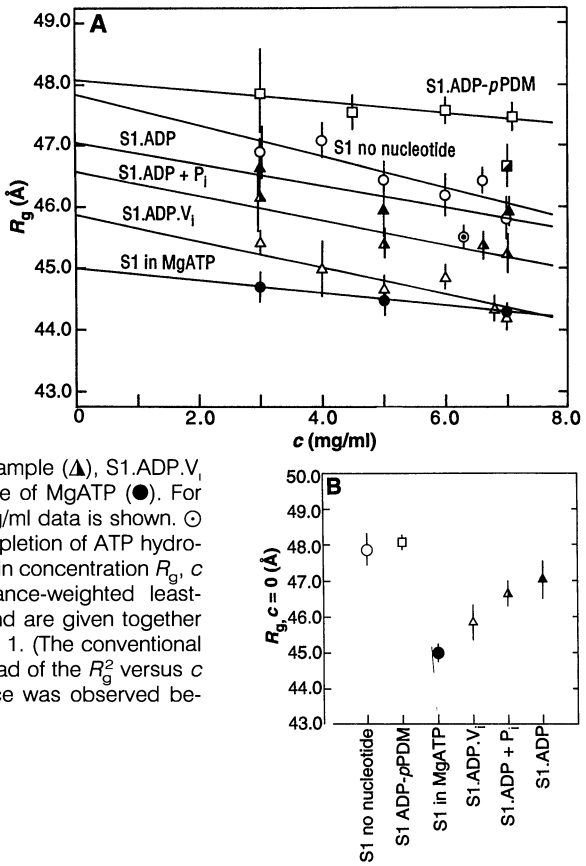

Fig. 2. Protein concentration dependence of the apparent R_g of various S1 samples (**A**). The R_g (the root-mean-square distance of the electrons from the center of gravity of the molecule) was calculated from the slope ($\sqrt{3}/2\pi \times \{\Delta \ln[I(S)]/\Delta S^2\}^{1/2}$) of the Guinier region as shown in Fig. 1. This region was chosen to produce a linear Guinier plot with low variance (*21*) that would not be affected by the shape of a molecule (*14, 15*). The Guinier region of the scattering data showed no more than one linear component. (Top to bottom) S1.ADP-*p*PDM complex (□), nucleotide-free S1 (○), S1.ADP complex (▲), S1.ADP + P_i sample (◮), S1.ADP.V_i complex (△), and S1 in the presence of MgATP (●). For S1.ATPγS (◪), only the value of 7 mg/ml data is shown. ⊙ denotes the R_g value of S1 after completion of ATP hydrolysis. The final R_g values at zero protein concentration R_g, $c = 0$) were determined by a variance-weighted least-squares fit (*32*) to the data points and are given together with associated SDs in (**B**) and Table 1. (The conventional R_g versus c plot was used here instead of the R_g^2 versus c plot because no significant difference was observed between them.)

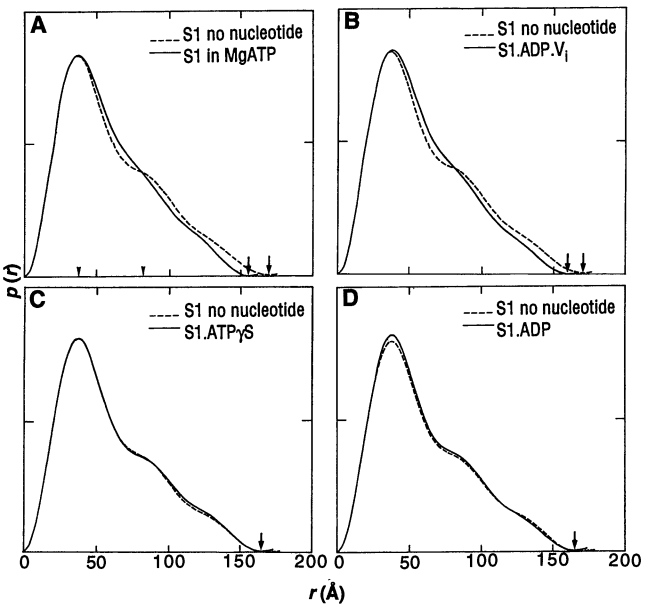

Fig. 3. Pair-distance distribution functions [$p(r)$ profiles] of four S1 samples. The function $p(r)$ denotes the frequency of vector lengths (r) connecting small volume elements within the entire volume of the molecule (*14, 15*). Each $p(r)$ profile is shown superimposed with that of the nucleotide-free S1 (the dashed line). (**A**) S1 in the presence of MgATP. (**B**) S1.ADP.V_i complex. (**C**) S1.ADPγS complex. (**D**) S1.ADP complex. The lack of a distinct shoulder around $r = 80$ Å in $p(r)$ functions of S1 in MgATP and S1.ADP.V_i together with the decrease in D_{max} shows that these complexes are compact (*15*). We calculated each $p(r)$ function by an inverse Fourier transformation of the average $I(S)/c$ data in the range $0 \le S \le S_o$, where S_o (= 0.0220 Å^{-1}) is the outer limit of the present small-angle scattering intensity measurement with a long camera length. The slightly oscillatory nature in $p(r)$ was due mainly to the termination effect. In the calculation, the extrapolated values of the straight line in the Guinier plot were used for $I(S)$ data in the region of $0 \le S \le S_{min}$. The $p(r)$ functions averaged from 3, 5, and 7 mg/ml data were shown, except for S1.ATPγS (data at 7 mg/ml only) [no significant concentration dependence was observed in $p(r)$]. The maximum chord length D_{max} of the molecule is defined as the distance at which the $p(r)$ function eventually drops to zero or as the r-intercept (*15*). The apparent D_{max} positions are depicted by arrows and the numerical values are listed in Table 1. The $p(r)$ function of the S1.ADP-*p*PDM complex (not shown) was similar to that of nucleotide-free S1 but gave a slightly larger D_{max} (see Table 1).

and beyond S^2_{max} the plots deviated upward from the straight lines because of the asymmetric shape of S1. The deviation of S1 in the MgATP solution was less than that of nucleotide-free S1, showing that the shape of S1 is more compact or less asymmetric in the presence of MgATP (*14, 15*). The deviation of the stable complex with ADP and vanadate (V_i) (S1.ADP.V_i) (*16*) was as small as that of S1 in the MgATP solution. In contrast, curves of an adenosine 5′-γ-thiotriphosphate–bound S1 (S1.ATPγS) (*17*), an S1 with MgADP trapped as a result of the cross-linking of Cys^{707} (SH_1) and Cys^{697} (SH_2) with *p*-phenylenedimaleimide (*p*PDM) (S1.ADP-*p*PDM) (*11, 18*; not shown) and an ADP-bound S1 (S1.ADP), deviated as much as the curve of nucleotide-free S1.

The apparent radius of gyration R_g can be calculated from the slope of straight lines in the Guinier plots (*14*) in the range of 0.0778×10^{-4} Å^{-2} (S^2_{min}) $\le S^2 \le S^2_{max}$ as a function of the protein concentration c (Fig. 2A). In all cases, R_g decreased linearly with increasing c, again indicating that S1 exists in a monodisperse form. The slight differences in the slope can be explained by interparticle interference effects (*14, 15*) among different S1 samples; this effect is much weaker for S1 in the presence of MgATP and S1.ADP-*p*PDM than for other samples. The narrowness of the Guinier region in S1 samples was due to the large size and asymmetric shape of the molecule, as confirmed by calculations in which the crystal image of S1 (*19*) was used (see below). The R_g values, extrapolated to zero protein concentration, are depicted in Fig. 2B and Table 1. The R_g of S1 in the MgATP solution was about 3 Å less than that of nucleotide-free S1. The R_g of the S1.ADP.V_i complex was slightly greater than that of S1 in the MgATP solution. On the other hand, the R_g value of the S1.ADP-*p*PDM complex was almost the same as that of nucleotide-free S1, and R_g for the S1.ADP complex was only very slightly smaller than that of nucleotide-free S1. The result with S1.ADP-*p*PDM is consistent with previous x-ray scattering data (*7*). After completion of ATP hydrolysis (*11*), the scattering curve and R_g value from the S1 sample were nearly identical to the ones from the S1.ADP + inorganic phosphate (P_i) sample (*11*) (and the S1.ADP complex) (see ⊙ in Fig. 2A). The magnitudes of R_g are sorted in the following order: S1 in MgATP < S1.ADP.V_i < S1.ADP + P_i ≅ S1.ADP < nucleotide-free S1 ≅ S1.ADP-*p*PDM, (Fig. 2B).

The R_g value of nucleotide-free S1 (47.8 Å) is significantly larger than the value previously obtained for papain-treated rabbit S1 (32.8 Å) from x-ray scattering (*20*). The difference is principally related to a

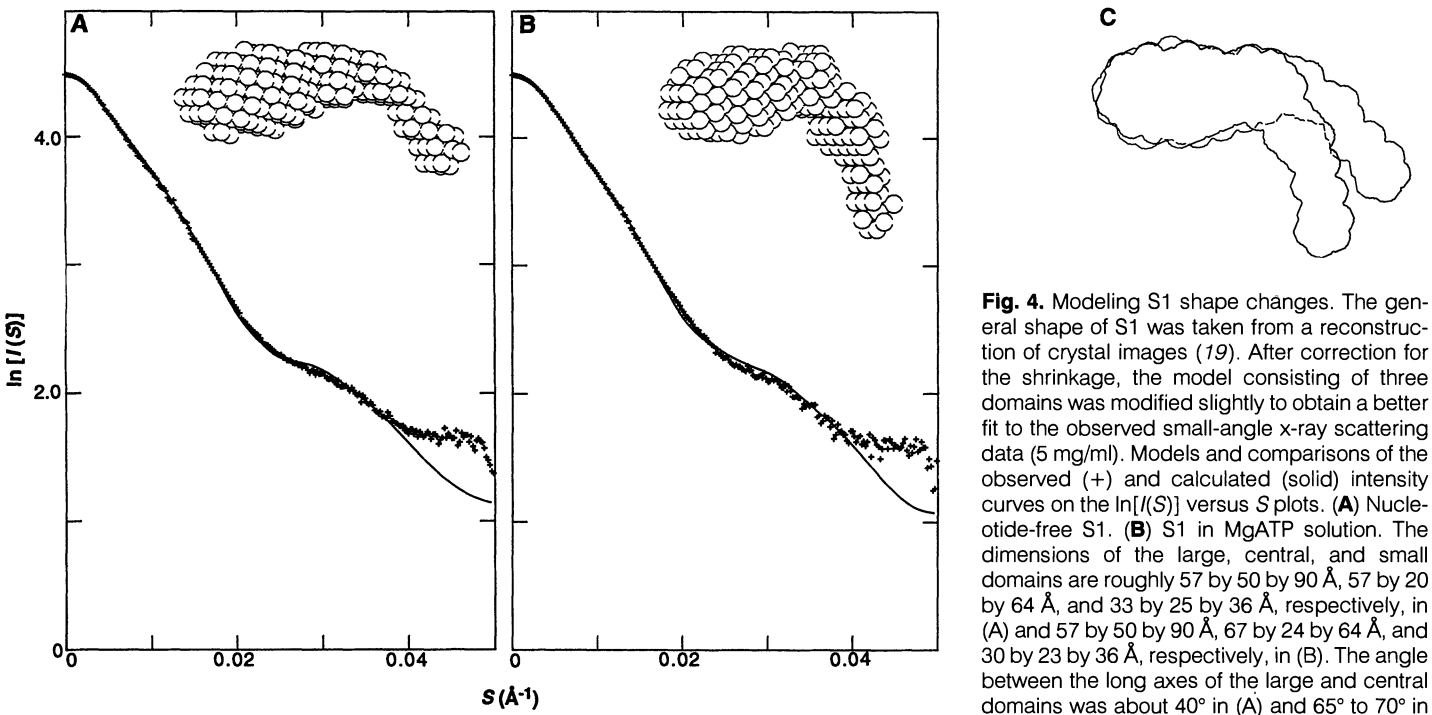

Fig. 4. Modeling S1 shape changes. The general shape of S1 was taken from a reconstruction of crystal images (*19*). After correction for the shrinkage, the model consisting of three domains was modified slightly to obtain a better fit to the observed small-angle x-ray scattering data (5 mg/ml). Models and comparisons of the observed (+) and calculated (solid) intensity curves on the ln[$I(S)$] versus S plots. (**A**) Nucleotide-free S1. (**B**) S1 in MgATP solution. The dimensions of the large, central, and small domains are roughly 57 by 50 by 90 Å, 57 by 20 by 64 Å, and 33 by 25 by 36 Å, respectively, in (A) and 57 by 50 by 90 Å, 67 by 24 by 64 Å, and 30 by 23 by 36 Å, respectively, in (B). The angle between the long axes of the large and central domains was about 40° in (A) and 65° to 70° in (B). The high-angle intensity data beyond S = 0.020 Å^{-1} in the observed curves are taken from the data that were obtained at 50 mg/ml with the shorter camera length and spliced to the 5 mg/ml data by a least-squares fitting procedure. Below S_{min} the extrapolated values of the Guinier straight line were used. (**C**) The two S1 moieties drawn superimposed on each other in outline form by placing the center of gravity of the large domain of the (B) model over that of the (A) model. The transition from (A) to (B) was made mainly by an increase of the angle between the long axes of the large and central domains by 25° to 30°, whereas the overall structure of each domain was preserved. The center of gravity of the small domain moves about 40 Å from its position of the nucleotide-free S1. In order to fit the observed intensity curves, it was necessary to introduce a small cavity with about 6% of its volume into the large domain and to alter the size of the central and small domains slightly in the transition from (A) to (B). The R_g values are 48 Å in (A) and 45 Å in (B). The intensity profiles from these models were calculated by Debye's equation (*14, 15*) with an aggregate of 10 Å–diameter spheres as shown in (A) and (B). At present much weight should not be placed on the difference between the calculated and observed intensity profiles beyond S = 0.025 Å^{-1}.

Table 1. Effect of nucleotide binding on the radius of gyration (R_g) and the maximum chord length (D_{max}) of the S1 molecule and its estimated molecular weight. The R_g values extrapolated to zero protein concentration (c = 0), and SDs of the straight line obtained by a variance-weighted least-squares fit (*32*) are given. For S1.ATPγS and ATP-depleted S1, the results from 7 mg/ml data are shown in parentheses. Note that the slightly larger D_{max} of the S1.ADP-*p*PDM complex may indicate a more extended shape than a nucleotide-free S1 (*28*).

Samples	R_g (Å) (c = 0)	D_{max} (Å)	Molecular weight (× 10⁴)
S1 no nucleotide	47.8 ± 0.4	167 ± 3	12.4 ± 0.9
S1 in MgATP	45.0 ± 0.1	155 ± 3	12.5 ± 0.9
S1.ADP.V_i	45.9 ± 0.5	156 ± 1	12.4 ± 0.7
S1.ADP-*p*PDM	48.1 ± 0.2	175 ± 4	12.9 ± 0.6
S1.ATPγS	(46.3 ± 0.1)	(164)	
S1.ADP	47.0 ± 0.5	163 ± 2	12.2 ± 0.3
S1.ADP + P_i	46.7 ± 0.4		13.0 ± 0.4
S1 ATP-depleted	(45.4 ± 0.2)		

difference in the S^2 region used in the determination of R_g (*21*). The region used in the previous studies (*20*) was 0.3 × 10^{-4} Å^{-2} ≤ S^2 ≤ 0.7 × 10^{-4} Å^{-2}, where the Guinier plot is much less steep (see Fig. 1). The range between 0.3 and ~0.7 × 10^{-4} Å^{-2} is far beyond the straight region of the present Guinier plots, and thus it was not the correct Guinier region of S1. Our R_g value is in agreement with the value recently obtained for papain-treated S1 preparation (46 ± 2 Å) by neutron scattering [almost the same S^2 region as ours was used (*22*)] and is comparable to the value estimated from the size of the myosin head determined by EM (*23*).

The zero-angle intensity [$I(0)/c$] versus c plot was linear. Extrapolation of this plot to zero protein concentration yielded a value of 126 kD (mean ± 6 kD SD) as the apparent molecular mass of S1 (*24*) (see Table 1), close to that of the present papain-treated S1 (*9*).

Pair-distance distribution functions $p(r)$ (where r is the real-space vector length) (*14, 15*) were calculated by an inverse Fourier transformation of the various S1 scattering data (Fig. 3). The $p(r)$ of nucleotide-free S1 had a peak at r = 37 Å and a distinct shoulder at r = ~80 Å (arrowhead in Fig. 3A). This asymmetric profile of $p(r)$ confirms that S1 is a highly elongated molecule with an asymmetrically decreasing cross section toward its end (*15*). The shoulder is indicative of the domain structure within an S1 molecule, its position corresponding to the interdomain distance (*15*). The r-intercept of $p(r)$ gave a maximum chord length (maximum internal particle dimension) D_{max} (*14, 15*) of about 167 Å. The $p(r)$ curve of S1 in the MgATP solution showed a peak at the same position, had a less distinct shoulder, and intersected the nucleotide-free S1 curve at r ~80 Å. Beyond this, there are significantly fewer vector lengths than in nucleotide-free S1, resulting in a D_{max} shorter by about 10 Å (see Table 1). The R_g values derived as the second moment of these $p(r)$ functions (*15*) agreed well with those from the Guinier analyses. The data

in Fig. 3, A and B, show that the conformations of S1 in the presence of MgATP and the S1.ADP.V_i complex are similar, except for a small difference in R_g (Fig. 2B and Table 1). However, Fig. 3, C and D, indicates that the conformations of the S1.ATPγS (or S1.ADP-*p*PDM) and S1.ADP complexes are rather similar to that of nucleotide-free S1.

These results show that the shape of S1 becomes compact (more round or bent) in the presence of MgATP, in agreement with the recent EM studies (*4*, 6). Among the elementary states of the S1 ATPase cycle, that of S1**.ADP.P_i is probably more compact than other states. This can be inferred because S1**.ATP.P_i is the predominant steady-state intermediate of the S1 ATPase cycle (*13*) and because the S1.ADP.V_i complex is an analog of the S1**.ADP.P_i (*25*) complex; furthermore, our data show that the S1.ADP.V_i complex also has a compact structure. The compact structure of the S1.ADP.V_i complex is consistent with the results of electric birefringence (*26*) and fluorescence anisotropic decay (*27*) studies. Thus, major changes are induced by ATP, leading to an altered conformation of the predominant intermediate, S1**.ADP.P_i.

The present results also indicate that the structure of S1 changes little after the initial binding of ATP, if it is assumed that the S1.ATPγS complex or the S1.ADP-*p*PDM complex, or both, are stable analogs of the S1-bound ATP transient state (*17, 18*). S1 returns to nearly its original structure after release of P_i or ADP. Thus, large shape changes of S1 should occur in the transition into the S1**.ADP.P_i state and in the product (possibly P_i) release step from S1**.ADP.P_i.

Recently, the structure of the same type of S1 sample (chicken pectoralis myosin S1) was deduced by conventional three-dimensional reconstruction of crystal images at ~25 Å resolution (*19*). In order to determine the extent of motions or the structural changes that would account for the changes of R_g and D_{max} observed here, we calculated S1 shape changes with the use of a model consisting of three domains from the crystal reconstruction by taking into account the changes of the whole scattering profiles (Fig. 4). The initial model had a curved, tadpole-like shape, which was modified slightly to fit the observed intensity curve (Fig. 4A). The 5 to 6% decrease in R_g and approximately 7% reduction in D_{max} of S1 in the MgATP solution could be explained mainly by rotation or bending by 25° to 30° between the long axes of the large and central domains in the nucleotide-free S1 model (Fig. 4B). Most of the overall structure of the domains was preserved, although the size of the central and small domains was altered slightly. The displacement of the center of gravity of the small domain was about 40 Å from its original position, where the center of gravity of the large domains in both models coincided with each other (Fig. 4C). Thus, the calculations reveal fairly large shape changes of S1 in the presence of MgATP. Although at present the models for the shape changes shown in Fig. 4 are not unique, we find it difficult to explain the observed changes in the scattering profiles without varying the degree of asymmetry of the molecule. More detailed analyses are needed to lead to a definite conclusion.

There may be other explanations. As suggested by ^{31}P nuclear magnetic resonance (*2*) and recent EM studies (*4, 28*), myosin exists as an equilibrium mixture of different conformations. This may be an alternative reason for the observed narrowness in the Guinier region (*14, 15*). In this case, the observed changes of x-ray scattering could come from a shift of the equilibrium. A recent mechanical and x-ray diffraction study on a contracting muscle fiber (*29*) revealed that multiple elementary force-generating processes are repeated during hydrolysis of one ATP molecule. This result also suggests that the myosin head in the active state is in equilibrium between at least two conformations. In any case, the proportion of S1 in a compact form would greatly increase in the active state.

Our most recent high-resolution scattering data obtained with an area detector (an imaging plate) [see, for example, (*30, 31*)] confirmed all of the results described here, and the change in the high-angle part also suggested an alteration in the internal structure of S1 in the presence of MgATP and the S1.ADP.V_i complex.

The present findings provide quantitative evidence that interaction with ATP is accompanied by substantial changes in the myosin head shape that are correlated with the key biochemical states of the S1 ATPase cycle. These structural changes of S1, together with the changes of actin, may be associated with an energy-transducing mechanism in the elementary force-generating process of muscle contraction as well as with in vitro motility of actomyosin.

REFERENCES AND NOTES

1. Y. Harada *et al.*, *Nature* **326**, 805 (1987); Y. Y. Toyoshima *et al.*, *ibid.* **328**, 536 (1987).
2. J. W. Shriver, *Trends Biochem. Sci.* **9**, 322 (1984); _____ and B. D. Sykes, *Biochemistry* **20**, 2004 (1981).
3. P. J. Vibert and C. Cohen, *J. Muscle Res. Cell Motil.* **9**, 296 (1988).
4. M. Tokunaga *et al.*, *Adv. Biophys.* **27**, 157 (1991).
5. R. Craig, L. E. Greene, E. Eisenberg, *Proc. Natl. Acad. Sci. U.S.A.* **82**, 3247 (1985).
6. E. Katayama, *J. Biochem. (Tokyo)* **106**, 751 (1989).
7. D. B. Stone and R. A. Mendelson, *Biophys. J.* **49**, 444 (abstr.) (1986).
8. P. M. G. Curmi, D. B. Stone, D. K. Schneider, J. A. Spudich, R. A. Mendelson, *J. Mol. Biol.* **203**, 781 (1988).
9. T. Maita *et al.*, *J. Biochem. (Tokyo)* **110**, 75 (1991).
10. S. S. Margossian, W. F. Stafford III, S. Lowey, *Biochemistry* **20**, 2151 (1981).
11. Preparation of myosin S1. Myosin was prepared from fresh chicken breast (pectoralis) muscle and mildly digested with papain (Worthington, Freehold, NJ) in the presence of Mg^{2+} at 20°C for 15 min to obtain S1 (*10*). Papain-digested S1 was further purified on a high-performance liquid chromatography (HPLC) gel filtration column (Superose 6, Pharmacia). Purified S1 was immediately used for x-ray experiments without freeze-drying. SDS–polyacrylamide gel electrophoresis of this preparation showed both classes of light chains and a heavy chain for a total molecular mass of about 130 kD (*9*). ATPγS (Boehringer Mannheim) was purified before use by HPLC ion-exchange chromatography. The composition of the standard buffer solution for x-ray scattering was 150 mM KCl, 0.5 mM dithiothreitol, and 10 mM imidazole-HCl (pH 7.0). Various nucleotide-bound S1 samples were made with the same preparation of S1. For preparing an S1.ADP.V_i complex (*16*), 0.5 mM ADP, 1.5 mM $MgCl_2$, and 0.5 mM vanadate (V_i) were added to the buffer solution. For measurements with ATP, ADP, or ATPγS, 5 mM nucleotide and 6 mM $MgCl_2$ were added to the S1 solution just before each x-ray experiment. The S1.ADP + P_i sample was prepared by addition of 5 mM P_i to the S1.ADP sample. The S1.ADP-*p*PDM sample was prepared by conventional procedures (*18*) and purified with a Superose 6 column after modification to remove any aggregated protein. The K^+-EDTA and Ca^{2+} ATPase activities (pH 8.0, 25°C) of purified samples were 0.44 and 1.5%, respectively, of the S1 activities (*12*), confirming that the S1.ADP-*p*PDM complex was cross-linked through SH_1 and SH_2. We made the ATP-depleted sample by allowing the S1-MgATP solution to hydrolyze 5 mM ATP overnight at 4°C. Protein concentrations were determined by absorbance at 280 nm with the use of $A^{1\%}_{280\ nm}$ = 8.3 cm^{-1}. Bovine serum albumin (BSA) (Sigma, A-0281), purified on the Superose 6 column, was used as a reference for x-ray measurements of S1 solutions.
12. Small-angle x-ray scattering measurements were performed with the use of a monochromatized x-ray beam (wavelength, 1.507 Å). Synchrotron radiation from a positron storage ring at the Photon Factory, Tsukuba, operated at 2.5 GeV with a ring current between 200 and 350 mA was selected and collimated with the double focusing optics [for recent status, see (*31*)]. In order to allow measurements at as small an angle as possible for the present experiments, we finely collimated the beam size at the specimen position to less than 1.0 mm (vertically) and 2.3 mm (horizontally) and took special care to minimize the parasitic scattering around the beam stop. The small-angle resolution of about 550 Å Bragg spacing was attained at a specimen-to-detector distance of 2.535 m. Scattered x-rays were recorded by a linear position-sensitive proportional detector (PSD) (Rigaku-Denki) or more recently on Fuji imaging plates (*30*). The PSD data were stored in a CAMAC memory linked to a Macro 11/F34 computer (ASR). The beam intensity incident at the specimen was monitored with an ion chamber placed in front of the specimen. The sample was contained in a temperature-controlled cell with mica windows, and the temperature was maintained at 18.5°C. Ten to 20 measurements for different samples were made on a single S1 preparation at different concentrations. Exposure time was set to 180 s to minimize radiation damage of the sample, although no appreciable indication of damage was detected in the x-ray scattering pattern from any of the samples up to exposures of at least 600 s. The ATPase activity of

S1 was measured after each x-ray experiment; the K^+-EDTA, Ca^{2+}, and Mg^{2+} ATPase activities were 15 (pH 8.0), 2.6 (pH 8.0), and 0.07 s^{-1} (pH 7.0), respectively, at 25°C. Buffer scattering measurements were performed periodically throughout the measurement sequence. The average count rates were 3,000 to 4,000 counts per second from buffer solution and 6,000 to 11,000 counts per second from sample solutions. After correction with the use of current values measured with the ion chamber, we obtained the net scattering intensity data $I(S)$ by subtracting the buffer scattering from the sample solution scattering. We performed similar measurements with solutions of BSA, assuring the validity of the S1 measurements very near to the beam stop. The data were analyzed on PDP11/34 (DEC) and SPARC Station 330 (SUN) computers.

13. C. R. Bagshaw *et al.*, *Biochem. J.* **141**, 351 (1974).
14. A. Guinier, *Small-Angle Scattering of X-Rays* (Wiley, New York, 1955).
15. O. Glatter, in *Small-Angle X-Ray Scattering*, O. Glatter and O. Kratky, Eds. (Academic Press, New York, 1981), pp. 119–196; L. A. Feigin and D. I. Svergun, *Structure Analysis by Small-Angle X-Ray and Neutron Scattering* (Plenum, New York, 1987).
16. C. C. Goodno, *Methods Enzymol.* **85**, 116 (1982).
17. R. S. Goody and W. Hofmann, *J. Muscle Res. Cell Motil.* 1, 101 (1980); M. A. Geeves and D. R. Trentham, *Biochemistry* **21**, 2782 (1982).
18. J. E. Wells and R. G. Young, *Methods Enzymol.* **85**, 93 (1982).
19. D. A. Winkelmann, T. S. Baker, I. Rayment, *J. Cell Biol.* **114**, 701 (1991).
20. K. M. Kretzschmar, R. A. Mendelson, M. F. Morales, *Biochemistry* **17**, 2314 (1978); R. A. Mendelson and K. M. Kretzschmar, *ibid.* **19**, 4103 (1980).
21. The radius of gyration of R_g must be determined in the range $0 \leq S^2 \leq (1/2\pi R_g)^2$ (the Guinier's criterion) or at least in the range where $S^2 = (1/2\pi R_g)^2$ (estimated with the use of the approximate R_g value of the molecule) is involved (*14, 15*). The size of the region (a Guinier region) over which this approximation holds depends not only on the size but also on the shape of the molecule in a monodisperse solution. Outside the Guinier region the scattering profile is mainly governed by the shape of the molecule. For a head portion (S1) of a myosin molecule, the R_g value has been estimated as ~46 Å from its molecular weight and size (*23*). By referring to this value, we used the region $[S^2_{min} (= 0.0778 \times 10^{-4}$ Å$^{-2}) \leq S^2 \leq S^2_{max} (= 0.2228 \times 10^{-4}$ Å$^{-2})]$ in the determination of R_g to produce a linear plot with low variance as shown in Fig. 1. The excellent linearity of the Guinier plots in the region below S^2_{max} shows that there are no appreciable aggregates such as dimers in any of the samples. The region $< S^2_{min}$ was not used because parasitic scattering around the beam stop influenced the data slightly.
22. R. A. Mendelson, D. Bivin, P. M. G. Curmi, D. K. Schneider, D. B. Stone, *Adv. Biophys.* **27**, 145 (1991).
23. A. Elliott and G. Offer, *J. Mol. Biol.* **123**, 505 (1978).
24. We estimated the molecular mass of S1 [partial specific volume 0.72 cm^3/g (*10*)] by linearly extrapolating the zero angle intensity $I(0)/c$ data of S1 samples and BSA (molecular mass 66.3 kD) to zero protein concentration (*14, 15*).
25. C. Wells and C. R. Bagshaw, *J. Muscle Res. Cell Motil.* **5**, 97 (1984).
26. S. Highsmith and D. Eden, *Biochemistry* **29**, 4087 (1990).
27. R. Aguirre, S.-H. Lin, F. Gonsoulin, C.-K. Wang, H. C. Cheung, *ibid.* **28**, 799 (1989).
28. M. Walker and J. Trinick, *J. Muscle Res. Cell Motil.* **9**, 359 (1988).
29. M. Irving, V. Lombardi, G. Piazzesi, M. A. Ferenczi, *Nature* **357**, 156 (1992).
30. Y. Amemiya *et al.*, *Top. Curr. Chem.* **147**, 121 (1988).
31. K. Wakabayashi and Y. Amemiya, in *Handbook on Synchrotron Radiation*, S. Ebashi, M. Koch, E. Rubenstein, Eds. (North-Holland, Amsterdam, 1991), vol. 4, pp. 597–678. [For the original paper of the present optics, see Y. Amemiya *et al.*, *Nucl. Instrum. Methods* **208**, 471 (1983)].
32. P. R. Bevington, *Data Reduction and Error Analysis for the Physical Sciences* (McGraw-Hill, New York, 1969).
33. We thank M. Sato for the program used in the calculation of the $p(r)$ function and for assistance; T. Miyanishi for the sequence data of chicken S1; T. Hiratsuka for discussions; and Y. E. Goldman for critical reading of the manuscript and valuable comments.

3 April 1992; accepted 15 July 1992

Neural Computing in Cancer Drug Development: Predicting Mechanism of Action

John N. Weinstein,* Kurt W. Kohn, Michael R. Grever, Vellarkad N. Viswanadhan, Lawrence V. Rubinstein, Anne P. Monks, Dominic A. Scudiero, Lester Welch, Antonis D. Koutsoukos, August J. Chiausa, Kenneth D. Paull

Described here are neural networks capable of predicting a drug's mechanism of action from its pattern of activity against a panel of 60 malignant cell lines in the National Cancer Institute's drug screening program. Given six possible classes of mechanism, the network misses the correct category for only 12 out of 141 agents (8.5 percent), whereas linear discriminant analysis, a standard statistical technique, misses 20 out of 141 (14.2 percent). The success of the neural net indicates several things. (i) The cell line response patterns are rich in information about mechanism. (ii) Appropriately designed neural networks can make effective use of that information. (iii) Trained networks can be used to classify prospectively the more than 10,000 agents per year tested by the screening program. Related networks, in combination with classical statistical tools, will help in a variety of ways to move new anticancer agents through the pipeline from in vitro studies to clinical application.

There are millions of different molecules that should be screened for their activity against cancer. Some are natural products collected from rain forests, oceans, and other habitats; some are products of synthetic organic chemistry. Before 1985, primary screening of new compounds was done in mice bearing the murine leukemia P388. It was not clear, however, that this screening would identify agents effective against solid tumors, including the common human carcinomas (*1*). An alternative possibility, disease-oriented primary screening against panels of in vivo tumors, would not have been feasible for the very large numbers of candidate compounds. These issues motivated development of the current National Cancer Institute (NCI) drug screening, in which compounds are tested in culture for their ability to inhibit the growth of a panel of 60 different human tumor cell lines (*1*). The cell lines in the panel represent a spectrum of histologies and organs of origin. The NCI screening program is currently testing several hundred compounds per week, including both synthetic and natural products.

Implicit in this screening strategy is the premise that agents tested will show reproducible patterns of differential response among these 60 cell lines. Paull *et al.* developed a computer program called COMPARE (*2*) to seek useful information in those patterns. For a designated "seed" compound, COMPARE searches the database of already tested agents for ones with the most similar patterns of activity against the cell panel. The pairwise comparisons are based on Pearson correlation coefficients. Early on it was noticed that compounds matched by pattern often had similar chemical structures. Further study indicated that the matches generally related to in vitro

J. N. Weinstein and V. N. Viswanadhan, Laboratory of Mathematical Biology, Division of Cancer Biology, Diagnosis and Centers, National Cancer Institute, Bethesda, MD 20892.
K. W. Kohn, Laboratory of Molecular Pharmacology, Developmental Therapeutics Program, Division of Cancer Treatment, National Cancer Institute, Bethesda, MD 20892.
M. R. Grever, Developmental Therapeutics Program, Division of Cancer Treatment, National Cancer Institute, Bethesda, MD 20892.
L. V. Rubinstein and A. D. Koutsoukos, Biometric Research Branch, Cancer Therapy Evaluation Program, Division of Cancer Treatment, National Cancer Institute, Bethesda, MD 20892.
A. P. Monks, D. A. Scudiero, L. Welch, Program Resources, Inc./DynCorp., National Cancer Institute/Frederick Cancer Research and Development Center, Frederick, MD 21702.
A. J. Chiausa and K. D. Paull, Information Technology Branch, Developmental Therapeutics Program, Division of Cancer Treatment, National Cancer Institute, Bethesda, MD 20892.

*To whom correspondence should be addressed at Laboratory of Molecular Pharmacology, Developmental Therapeutics Program, Division of Cancer Treatment, National Cancer Institute, Building 37, Room, 5C-25, 9000 Rockville Pike, Bethesda, MD 20892.